IEEE Access
Multidisciplinary | Rapid Review | Open Access Journal

Received 30 January 2024, accepted 21 February 2024, date of publication 26 February 2024, date of current version 1 March 2024.

Digital Object Identifier 10.1109/ACCESS.2024.3369908

RESEARCH ARTICLE

Design and Analysis of the M3Rob: A Robotic Platform for Wrist and Hand Rehabilitation

GONZALO ALONSO-LINAJE, ANA CISNAL, (Graduate Student Member, IEEE), JUAN CARLOS FRAILE, AND JAVIER P. TURIEL

Instituto de Tecnologías Avanzadas de la Producción (ITAP), University of Valladolid, 47011 Valladolid, Spain

Corresponding author: Ana Cisnal (cisnal@ieee.org)

This work was supported in part by the Ministry of Science and Innovation under Project RTC2019-007350-1, and in part by Company TICCYL Digital S.L.

ABSTRACT Physical therapy plays a crucial role in the motor recovery. Rehabilitation robots have emerged as significant advancement, enabling repetitive therapeutic interventions in both clinical and home settings. In this context, the development of a highly functional, reliable, portable, and cost-effective mechatronic systems for wrist and hand rehabilitation represents a significant step in the field. This article focused on the design and implementation of the M3Rob device, a 3-DoF wrist exoskeleton equipped with a force sensor, allowing for the execution of active therapies, recognized for their effectiveness in motor recovery. Hence, a close-loop admittance control utilizing a joint-space target trajectory as input is presented and experimentally evaluated across three distinct levels of assistance. Moreover, to address the need for rehabilitation targeting activities of daily living, the device enables the incorporation of a hand exoskeleton for simultaneously performing hand and wrist rehabilitation. Featuring a range of motion of 180° for pronation/supination, 120° for flexion/extension, and 75° for ulnar/radial deviation, in combination with joint torques spanning from 7.85 to 43.86 Nm, the device covers the required motions and forces essential for daily activities. The presented device offers a comprehensive solution for wrist and hand rehabilitation, effectively addressing critical challenges in motor recovery.

INDEX TERMS Admittance control, assistive robots, dynamics, kinematics, mechanical design, mechatronics, wrist rehabilitation exoskeleton.

I. INTRODUCTION

The hand, characterized by its intricate kinematic capabilities, enables interaction with the environment through grasping and touching actions, and the wrist, a complex articulation facilitating hand positioning and manipulation in space. Wrist and hand are collectively indispensable for executing activities of daily living (ADLs), work-related tasks, and recreational activities. However, individuals affected by central nervous system (CNS) injuries, including stroke, and traumatic brain injury [1], or musculoskeletal disorders (MSDs), such as fractures, or arthritis [2], [3], may experience motor impairments in the hand and/or wrist, resulting in weakened movements, pain, limited range of motion, and diminished functionality [4].

In such cases, the rehabilitation of the wrist and hand is crucial for restoring motor function, preventing complications, and alleviating pain, ensuring individuals regain functional independence and proficiency in daily tasks reliant on these essential joints, like grasping objects, typing, and various fine motor skills [5]. Various modalities, including manual therapy, exercises, orthoses, physical agents, education, and counseling, can be incorporated into rehabilitation strategies. In the realm of physical therapies, mechatronic devices have been developed to assist patients in performing repetitive wrist and hand movements, thus facilitating the rehabilitation process for healthcare personnel [6]. One of the major challenges is the development of a device capable of assisting a

The associate editor coordinating the review of this manuscript and approving it for publication was Guilin Yang.

comprehensive range of motion (ROM), including all three wrist rotations, as well as independent finger flexion and extension.

Wrist rehabilitation exoskeletons are typically composed of complex mechanical structures and multiple actuators to assist wrist movements. Over the past few decades, numerous proposals have emerged. Despite the diversity of proposed configurations, the current trend is towards compact and portable devices. Rice University (Houston, TX, USA) has developed wrist rehabilitation robots such as MAHI [7], RiceWrist [8], MAHI EXO II [9], RiceWrist-S [10], and OpenWrist [11]. The MAHI, RiceWrist, and MAHI EXO II devices consist of a parallel mechanism system to assist in the rotational movements of the wrist, and both MAHI and MAHI EXO II also support elbow rehabilitation. Later, RiceWrist-S and OpenWrist robots were developed, featuring a more compact and rigid design that can incorporate a hand exoskeleton using the Readapt module [12].

Lincong Luo et al. [13] developed a wrist rehabilitation module with an adjustable plate to move the device handle according to the patient's arm size. Capello et al. [14] employed linear actuators instead of rotational motors to assist the three wrist DoFs. IIT wrist robot [15] is characterized by a compact design along with the RiceWrist-S and inspired the development of the Wrist Gimbal [16], a portable rehabilitation robot that assists in the 3 DoFs of the wrist. POWROBOT [17] has recently developed a portable device for 3-DoF wrist rehabilitation that incorporates a force sensor. Likewise, the robot presented by Gopura and Kiguchi [18] also used a force sensor. Nu-Wrist [19] is a 3-DoF rehabilitation robot that uses servo motors and 3D-printed parts.

The integration of combined wrist and hand rehabilitation in therapy sessions offers significant benefits [20] by closely emulating the movements required for activities of daily living. However, the development of mechatronic devices capable of supporting both functionalities remains limited due to the inherent mechanical design complexities. Among the few available solutions, the OpenWrist [11] device, in combination with the Readapt module [12], stands out as an integrated system capable of addressing this challenge. Another noteworthy device is the WRES [21], which offers a comprehensive upper limb rehabilitation capability.

On the other hand, extensive evidence has demonstrated the substantial enhancement of rehabilitation outcomes through the implementation of active therapeutic approaches. This is primarily attributed to the active participation of the patient, which promotes neural plasticity and motor learning [22]. In active therapies, the patient interacts with the rehabilitation device, hence intentionality detection is required [23]. Although various methods exist for detecting patient intentionality, one commonly employed involves the integration of a force sensor for measuring the exerted forces. However, the inclusion of a force sensor within the device introduces increased complexity. As a result, only a limited number of robotic systems described in the literature incorporate a force sensor, such as POWROBOT [17] and the one developed by Gopura and Kiguchi [18].

This article presents the M3Rob wrist device, a 3-DoF wrist rehabilitation robot, characterized by a wide range of motion (ROM) and portable design. It offers simultaneous rehabilitation of both hand and wrist through the integration of a hand rehabilitation exoskeleton. Moreover, the device is equipped with a force/torque (F/T) sensor to facilitate active therapy intervention. The article initially describes the mechanical design and hardware configuration. Subsequently, the kinematic and dynamic models of the robot are detailed, and a close-loop admittance control paradigm is implemented and evaluated. Finally, a comparative analysis of the features of the M3Rob wrist device and other related works is conducted to highlight the advantages of the proposed design.

II. DESIGN OF THE REHABILITATION ROBOT

A. SYSTEM REQUIREMENTS

The rehabilitation robot must be applicable to adults with upper limb impairments on either right or left side. The device should be 3-DoFs so it can assist on the rehabilitation of the pronation/supination (P/S) movement of the forearm and flexion/extension (F/E), and radial flexion/ulnar flexion (R/U) of the wrist. Additionally, the device must support the simultaneous rehabilitation not only the aforementioned 3 DoFs (P/S, F/E, and R/U), but also the mobility of the hand fingers.

The ROM should encompass the complete range observed in a healthy wrist or, at the very least, offer the essential ROM for executing ADLs. Table 1 presents the ROM for the three wrist rotation axes in healthy individuals determined by various sources, revealing some differences between the reported values. Table 1 also shows the ROM required to perform ADLs [24].

TABLE 1. Comparative evaluation of the ROM for wrist rotation axis in healthy individuals and ROM essential for ADLs.

Joint	P/S		F/E		R/U	
	Limits (°)	ROM (s)	Limits (°)	ROM (s)	Limits (°)	ROM (s)
Andrews et al. [25]			[35, -45]	80	[20, -18]	38
Yin-yu et al. [26]		150		114		70
Nizamis et al. [27]	[95, -42]	137	[75, -71]	146	[27, -40]	67
Perry et al. [28]		150		115		70
Ryu et al. [29]			[54, -60]	114	[17, -40]	57
ADLs [24]	[87, -77]	164	[74, -54]	128	[19, -13]	32

Additionally, to ensure proper cortical activation, it is essential that the robot supports performing slow repetitive movements within the physiological speed of a healthy wrist [30]. The average angular velocity values of the wrist during ADLs lie within the range of 20 to 40°/s, which is dependent on the type of the movement [31].

For the exoskeleton design, consideration must also be given to the torques required for each joint. Wrist stiffness was investigated in ten young and healthy individuals, revealing average values of 0.25/0.20 Nm for P/S movements, 0.66/0.16 Nm for F/E, and 2.01/1.21 Nm for R/U [7]. Additionally, during ADLs, a torque of 0.35 Nm is necessary for flexion/extension (F/E) and radial/ulnar deviation (R/U) movements, while slow pronation/supination (P/S) movements demand up to 0.06 Nm [21].

The robotic platform should be portable, and ergonomic to ensure its suitability in both home and clinical settings. Additionally, studies have revealed that active-assistive robotic systems may induce anxiety in certain patients [32], leading to the pursuit of a compact design that minimizes patient enclosure and facilitates the easy removal of the upper limb. The device must prioritize user safety by limiting the ROM and maximum speed to healthy wrist limits.

The effective execution of active rehabilitation therapies necessitates not only accurate position feedback but also precise measurements of force and torque. Consequently, the integration of a F/T sensor into the device is imperative. The optimal placement for the F/T sensor is the handle, as it serves as the primary application point for forces and torques exerted by the user. The F/T sensor must be compact to align with the geometrical characteristics of the robotic platform, ensuring an ergonomic, and optimal design.

B. SYSTEM OVERVIEW

The device features three serial revolute active joints (3-DoF RRR) to assist the pronation/supination (P/S), flexion/extension (F/E), and (radial flexion/ulnar flexion) R/U movements independently, and their axes are located at the center of the wrist. This design choice is based on the assumption that the metacarpals-carpal joint is rigid, thus justifying the use of a Cartesian coordinate system centered at the wrist midpoint for enhanced device performance.

The P/S movement involves the rotation of the carpus and radius around the ulna, whereas F/E, and R/U refer to rotations of the carpus around the radius. Due to its small size, the metacarpophalangeal joint can be considered rigid, simplifying the wrist modeling. This assertion was tested by Patterson et al. [33], who measured the difference between the angle formed by the third metacarpal and the radius, and that formed between the capitate and the radius during F/E movements. The average difference between these angles was $1.1 \pm 1.6°$, with a maximum of 4°. Consequently, the joint formed between the metacarpals and carpal bones can be considered as rigid [29].

In addition to the 3 active DoFs, the device has one passive prismatic DoF consisting of a forearm support guide to enable the adjustment of the device to the individual needs of each patient. The mechanical structure comprises a base (depicted in blue, Fig. 1) and three distinct rigid bodies: the green, red, and white bodies in Fig. 1 correspond to the P/S, F/E, and U/R movements, respectively. Notably, the white body incorporates a handle that serves as the interface between the device and the user.

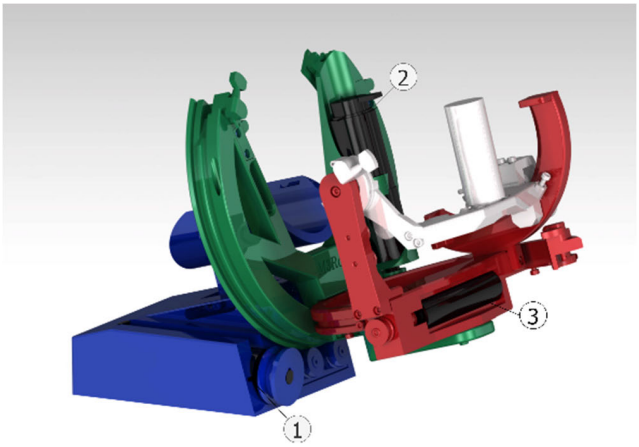

FIGURE 1. CAD model of the M3Rob wrist robot, indicating the four rigid bodies.

C. DEVICE SPECIFICATIONS

1) RANGE OF MOTION

Utilizing a compact design rooted in a 3-DoF RRR configuration, the M3Rob device covers the entire ROM characteristic of a healthy wrist (Table 1). It offers a P/S movement within limits of [90, −90] ° and a ROM of 180°. For F/E movement, the device allows motion within limits of [75, −45] ° and a ROM of 120°. Additionally, U/R movement is facilitated with limits of [35, −40] ° and a ROM of 75°.

Since the device must be applicable to individuals with upper limb impairments on either right or left side, attention must be paid to the fact that the ROM required for the F/E movements are different (75° for flexion and 45° for extension, as depicted in Table 1). Consequently, a mobile handle mechanism with a circular guide was designed to shift the TCP of the wrist platform by an angle of 30 ° (Fig. 2), thus enabling complete rehabilitation of both rotational movements independently of the limb undergoing rehabilitation.

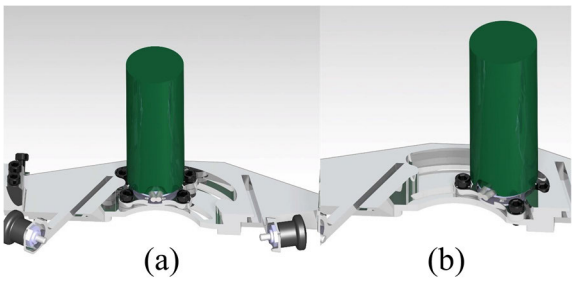

FIGURE 2. Circular guide for handle displacement. (a) Position for the right hand. (b) Position for the left hand.

The passive prismatic DoF enables a movement range of up to 28 mm, which is sufficient to accommodate the variation in size of the combined hand and forearm of the adult population, ensuring a comfortable fit in the forearm support. The

safety of the subject is ensured by several mechanical stops to limit the movement of each rigid body attached to the shaft of the motors (Fig. 3).

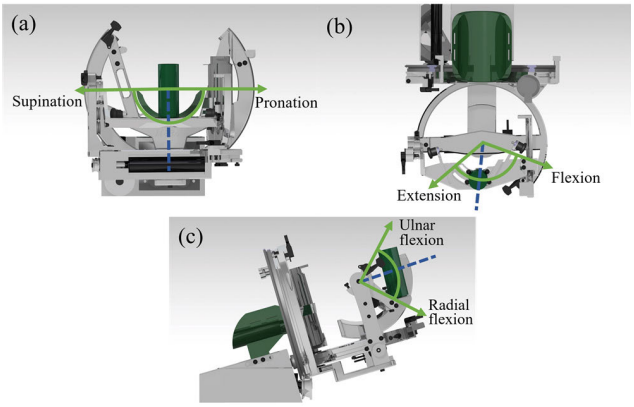

FIGURE 3. ROM limited by the mechanical stops for (a) P/S, (b) F/E, and (c) U/R movements.

2) ACTUATION SUB-SYSTEM

Three Maxon RE-series DC brushless motors, each equipped with a gear and encoder, and controlled by an ESCON Module 50/5 (Maxon Motor, Switzerland), are responsible for the actuation in the system (Table 2).

TABLE 2. Motor, gear and encoder specifications for the M3Rob platform.

Joint	Motor			Gear		Encoder	
	Model	Max Torque (Nm)	Max Speed (rpm)	Model	Reduction	Model	Resolution (ppv)
1-P/S	RE-40 (148877)	0.187	7590	GP 42 C (203117)	19: 1	MR, type L (225787)	1024
2-F/E	RE-40 (148877)	0.187	7590	GP 42 C (203117)	19: 1	MR, type (225787)	1024
3-R/U	RE-30 (310009)	0.0897	8490	GP 32 A (166162)	28: 1	HEDS 5540 (110511)	500

The motors are located so as to minimize gravitational and inertial loading, hence facilitating the corresponding independent axis movement and also to protect them from external agents. The remote placement of the actuators has led to the employment of a cable routing/guidance system to transmit the actuation to the joints, which is a reliable solution if the cable tensioning is correct. Therefore, worm gear sets are incorporated to facilitate the pretensioning of the transmission system, which utilizes a 1.5mm thick braided stainless-steel cable with a breaking tension of 1570 N/mm^2.

Since the P/S axis supports the entire weight of the structure, a R25255360 capstan ring (Hepcomotion, Netherlands) together with the FCC25255LBNS bearing carriage (Hepcomotion, Netherlands) is incorporated to facilitate the cable guidance of this axis. Conversely, the FE and RU movements, which experience fewer loads, are supported by axial bearings. The cable routing mechanism serves as dual purpose of allowing for the remote placement of the motor as well as achieving a transmission ratio (TR), which results in higher torque output and increased encoder resolution at the expense of a reduced speed (Table 3).

TABLE 3. Transmission ratio, maximum continuous joint torque output, maximum speed, and sensor resolution for the M3Rob platform.

Joint	TR	Output torque (Nm)	Output speed (°/s)	Sensor resolution (°/counts)
1 - P/S	6.8:1	24.16	352.45	$6.80 \cdot 10^{-4}$
2 - F/E	12.9:1	43.86	185.80	$3.58 \cdot 10^{-4}$
3 - R/U	3.16:1	7.85	575.72	$4.07 \cdot 10^{-3}$

The output parameters of the M3Rob robot, encompassing both speed and torque, surpass the parameters found in the literature. Although the M3Rob wrist device features configurable speed, for safety reasons, an upper limit of 40°/s is set through software.

3) FORCE/TORQUE SENSOR

The selection of the K6D27 50N/1Nm F/T sensor (Me&Systeme, Germany) with a GSV-8DS amplifier (Me&Systeme, Germany) for integration into the device stems from its capabilities and small size. The 6-axes F/T sensor, with size Ø27 mm × 25 mm, is strategically positioned under the handle to measure force for F/E and U/R deviation movements, as well as torque for P/S movement. The F/T sensor has a maximum capacity of 50 N in the X and Y axes, 200 N in the Z axis, and a maximum torque of 1 Nm in all three axes.

4) INTEGRATION OF A HAND EXOSKELETON

One of the most noteworthy features of the M3Rob wrist device design is its capability to offer individual wrist rehabilitation or simultaneous rehabilitation of both the hand and wrist. The M3Rob wrist device enables the integration of the RobHand (Fig. 4.a), a robotic exoskeleton for hand neuromotor rehabilitation [34], [35]. It allows hyperextension and flexion angles of up to 2° and 78°, respectively, for the metacarpophalangeal (MCP) joints [36].

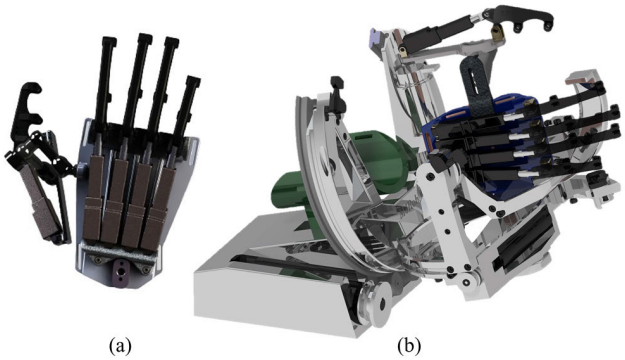

FIGURE 4. The RobHand exoskeleton for hand rehabilitation (a) CAD model (b) Assembly onto the M3Rob device.

A mechanism for retail assembly with a spring-loaded positioning anchor enables coupling RobHand to the wrist platform (Fig. 4.b). The support-plate of the RobHand exoskeleton has an L-shaped male component that restricts

movement in the transverse plane when coupled with the female rail of the wrist rehabilitation platform. Finally, the spring-loaded positioning anchor fully secured the coupling.

D. 3D-PRINTED PROTOTYPE

Manufactured using 3D printing techniques and PLA and ABS materials (Fig. 5), the device weighs less than 6 kg. The upper limb receives support from a specifically shaped element designed for the forearm, providing ergonomic and comfortable support. The exoskeleton is user-friendly, allowing easy use and removal. Users can simply grasp the handle and position their forearm in the support for wrist rehabilitation (Fig. 5a). In the context of combined hand and wrist rehabilitation, individuals need to wear the hand exoskeleton, subsequently position their forearm in the support, and secure the hand exoskeleton onto the wrist module (Fig. 5b). The forearm support includes two Velcro straps for adjustment if required based on the patient's condition. Additionally, the 6 kg exoskeleton is portable, offering stability without the need for fixation to a specific location. Installation is straightforward, requiring placement on a table or any horizontal surface.

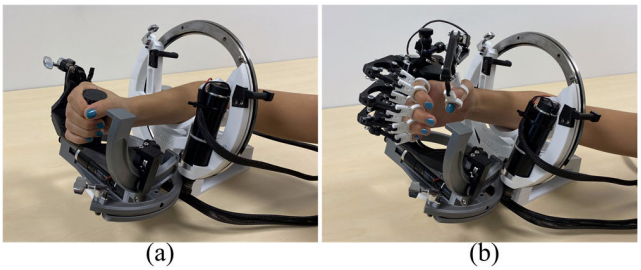

(a) (b)

FIGURE 5. 3D-printed M3Rob rehabilitation platform. (a) Only wrist rehabilitation. (b) Simultaneous wrist and hand rehabilitation.

III. MOVEMENT ANALYSIS

In this section, the kinematic and dynamic models of the M3Rob wrist device rehabilitation are presented.

A. KINEMATIC MODEL

The kinematic model of the robot is necessary for trajectory planning in the cartesian space. Therefore, a kinematic model is determined to compute the position and orientation of the Tool Center Point (TCP), which corresponds to the handle, relative to the base frame, given a set of motor joint angles. The robot uses three motors to individually assist one wrist rotation. According to 1, each motor angle (φ_i) is related to one individual wrist rotation (φ_i) through the corresponding transmission ratio (TR_i), previously specified in Table 2.

$$\varphi_i = \theta_i TR_i \tag{1}$$

The kinematic model of the robot is established by applying the matrix method introduced by Jacques Denavit and Richard Hartenberg (DH). The assignment of the coordinate frames of the links according to the DH convention and the joint-link parameters are illustrated in Fig. 6 along with the DH parameters of the model. The link length L1 represents the distance between the patient 's elbow and the wrist, which is 220±14 mm. Meanwhile, the link length L2 corresponds to the distance between the wrist center and the handle, measuring 65 mm.

Joint i	d_i	θ_i	a_i	α_i
1	L_1	$90°+\theta_1$	0	90°
2	0	$270°+\theta_2$	0	90°
3	0	$180°+\theta_3$	L_2	180°

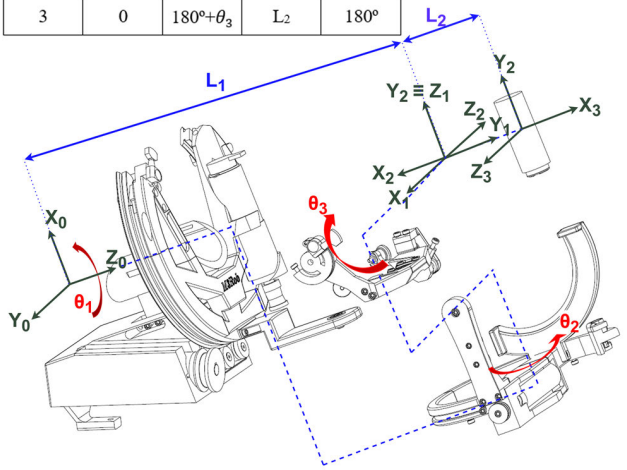

FIGURE 6. The coordinate frames associate to the links, geometrical and DH parameters.

The resulting DH matrix (T_0^{TCP}), which correlates the wrist angles (θ_i) with the rotation and translation of the TCP relative to the base frame, is provided in 2, as shown at the bottom of the next page, where S_i and C_i are the sine and cosine of the i-th degree of freedom.

B. DYNAMIC MODEL

The dynamic model establishes the relationship between the robot motion (position and its derivatives, velocity, and acceleration) and the applied forces and torques, based on dimensional parameters, such as link length, mass, and inertia. The Langrange-Euler method is used to determine the dynamic model of the M3Rob wrist device, which is expressed in 3 as a set of differential equations, where L_i represents the Lagrangian function, θi denotes the joint angle, $\dot{\theta}_i$ is the time derivative of θ_i, and τ_i denotes the non-conservative (external or dissipative) generalized forces performing work on the joint i.

$$\frac{d}{dt}\left(\frac{\partial L_i}{\partial \dot{\theta}_i}\right) - \frac{\partial L_i}{\partial \theta_i} = \tau_i \tag{3}$$

The Lagrangian function (L_i), which is dependent on the kinetic energy (K_i) and the potential energy (U_i), is expressed in 4.

$$L\left(\theta_i, \dot{\theta}_i\right) = K\left(\theta_i, \dot{\theta}_i\right) - U_i(\theta_i) \tag{4}$$

The computation of the kinetic energy (K_i) of a rigid body i is performed by 5, where m_i is the mass, v_i is the translational velocity of the center of mass, and I_i is the inertia. The

TABLE 4. Dynamic model parameters for the wrist robot with and without the hand exoskeleton.

Joint	Mass, m_i (kg)		Link length, l_i (mm)		Static friction, $F_{sf,i}$ (Nm)		Dynamic friction, $F_{df,i}$ (Nm)		Inclination, α_i (°)
	With hand	Without hand	With hand	Without hand	With hand	Without hand	With hand	Without hand	
1 - P/S	4.8	5.4	119	113	16	0.13	0.18	0.13	16
2 - F/E	2.6	3.2	86	85	74	0.35	0.52	0.44	74
3 - R/U	0.9	1.5	61	73	16	0.17	0.32	0.24	16

potential energy, defined by 6, depends on the mass (m_i), gravity (g), and height (h_i).

$$K_i\left(\theta_i, \dot{\theta}_i\right) = \frac{1}{2} m_i v_i^2 + \frac{1}{2} I_i \dot{\theta}_i^{\,2} \tag{5}$$

$$U_i\left(\theta_i\right) = m_i g h_i \tag{6}$$

The presence of attached bodies with varying positions introduces complexity to the determination of the dynamic model. Hence, an analysis of independent movements has been conducted, which simplifies the problem and provides a highly accurate approximation of the actual dynamic equations of motion. Consequently, for the model analysis of each body, the other solids are positioned at their initial positions, where all wrist angles are set to 0°, as this choice minimizes error due to weight and element position. Additionally, a simplified link model with concentrated mass is employed to calculate the inertias of rotating solids. Hence, by applying 3, the simplified dynamic model can be derived:

$$\tau_i\left(\theta_i\right) = m_i l_i^2 \ddot{\theta}_i + m_i g l_i \cos\alpha_i \, sen\,\theta_i \tag{7}$$

where α_i represents the inclination of the body i relative to the horizontal plane. Additionally, τ_i can be expressed as 8, which represents the summation of the motor torque (τ_m), external force exerted by the user on the exoskeleton (τ_{ext}), dynamic friction (τ_{df}), and static friction (τ_{sf}).

$$\tau_i = \tau_{m,i} - \tau_{ext,i} - \tau_{df,i} - \tau_{sf,i} \tag{8}$$

By combining 7 and 8, the motor torque can be determined as shown in 9.

$$\tau_{m,i}\left(\theta_i\right) = m_i l_i^2 \ddot{\theta}_i + m_i g l_i \cos\alpha_i \, sen\theta_i - Fe_i J^T\left(\theta_i\right) + F_f(\theta_i) \tag{9}$$

where Fe_i is the force exerted by the user at the TCP, J^T is the transpose of the Jacobin matrix of the system, and F_f is the summation of the dynamic friction (F_{df}) and static friction (F_{sf}).

To assess the static friction characteristics of each joint, a series of position ramps were executed throughout their respective ranges of motion (ROMs). To mitigate disturbances and isolate nonrigid body effects, the device was carefully oriented to align the axis of the targeted joint parallel to the gravitational direction. The other two joints were fixed using a high proportional gain PD controller, and the passive prismatic joint was securely immobilized. The ramp methodology employed in this study follows the same approach as described in [10], where the input ramps smoothly increase or decrease by 5° over a 2-second interval, followed by a 2-second pause, and continue in this pattern across the entire ROM (Fig. 7.a). Static friction values were deduced from the commanded current at the onset of movement, utilizing a soft proportional controller ($K_p = 0.2$). Fig. 7.b illustrates the static friction profile as a function of the joint angle. The mean and standard deviation of the static friction were found to be 0.16±0.05, 0.49±0.09, and 0.20±0.05 for the P/S, F/E, and R/U joints, respectively. Dynamic friction was quantified considering that the system behavior is that of an underdamped system, and achieved by analyzing the step response exhibited by each individual joint. The parameters required for calculating the dynamic model of each joint are provided in Table 4. It should be noted that two distinct dynamic models can be derived based on whether the hand exoskeleton is integrated into the device or not.

IV. ADMITTANCE CONTROL

Considering the characteristics of the mechatronic device, a closed-loop admittance control is designed using the information provided by the F/T sensor located at the human-robot contact point [37]. The proposed closed-loop admittance control (Fig. 8) utilizes the joint-space target trajectory (q_{ti}) as input. It comprises an outer loop responsible for computing the position setpoint of each joint (q_{ri}) through the admittance model (Y), and an inner position loop based on a PID controller. In the outer loop, the transpose of the Jacobian matrix ($J_g{}^T$) is employed to transform the forces (f_x, f_y, f_z) and torques (τ_x, τ_y, τ_z) applied by the patient at the TCP, measured by the F/T sensor, into resulting torques applied at each robot joint (τ_i). Once these torques are determined, the position increment of each joint (Δq_i) is determined using the mechanical admittance (Y). The internal control loop, featuring a PID controller with a conditional integrator to prevent

$$T_0^{TCP} = \begin{bmatrix} S_1S_2C_3 - C_1S_3 & S_1S_2S_3 + C_1C_3 & -S_1C_2 & L_2(S_1S_2C_3 - C_1S_3) \\ -C_1S_2C_3 - S_1S_3 & -C_1S_2S_3 + S_1C_2 & C_1C_2 & L_2(-C_1S_2C_3 - S_1S_3) \\ C_2C_3 & C_2S_3 & C_1C_2 & L_1 + L_2C_2C_3 \\ 0 & 0 & 0 & 1 \end{bmatrix} \tag{2}$$

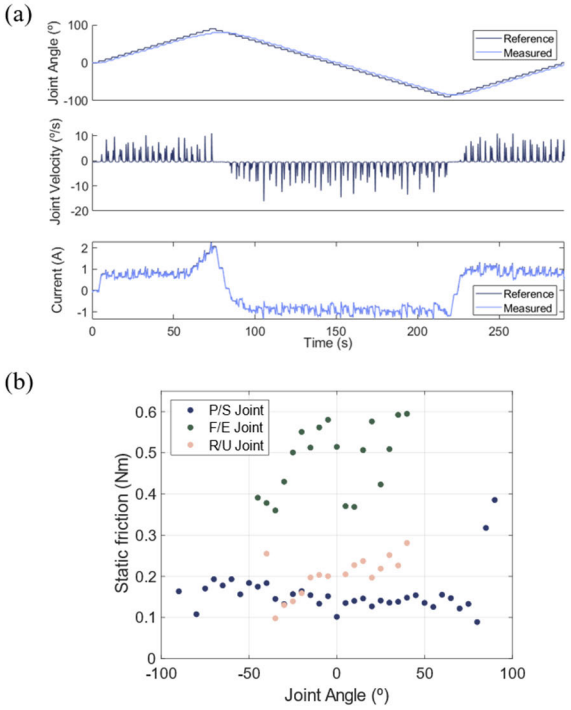

FIGURE 7. Determination of the static friction through the ramp tests. (a) Reference and measured position (up), measured velocity (middle), and reference and measured current (down) of the P/S joint during the test. (b) Static friction of the P/S, F/E, and R/U joints within their respective ROMs.

the windup phenomenon, calculates the torque required for the motors (τ_{ui}) given the position reference (q_{ri}) and the current position (q_i).

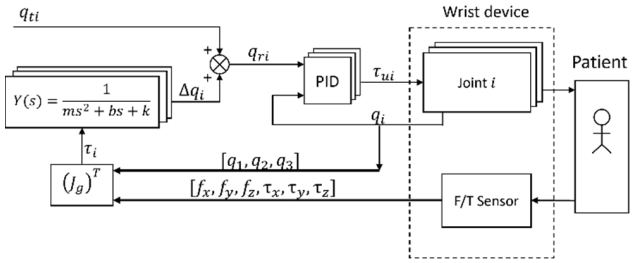

FIGURE 8. Close-loop admittance control using the joint-space target trajectory of the robot as reference.

The mechanical admittance variables (k, b, m) govern the amount of assistance of the wrist robot. Three distinct levels of mechanical admittance, representing high, medium, and low assistance, were experimentally determined to ensure stable control. Tests were conducted at each assistance level with a reference trajectory outlining a square with sides corresponding to 60° of F/E (q_2) and R/U (q_3) rotations (Fig. 9). Given six waypoints, the reference trajectory was computed using a trapezoidal velocity profile, with a maximum speed set at 20°/s. The participant deliberately refrained from exerting effort to adhere to the reference trajectory. As mechanical admittance varied, the actual trajectory exhibited noticeable patterns. While a reduction in admittance resulted in a more pronounced alignment of the actual trajectory with the

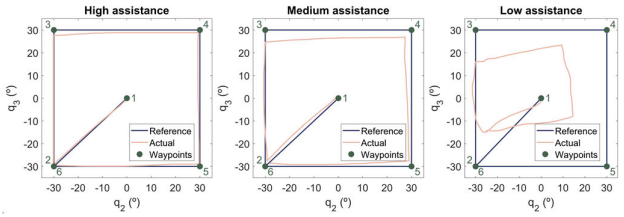

FIGURE 9. Evaluation of the closed-loop admittance control at three assistance levels: high, medium, and low. A healthy subject made no effort to follow the reference trajectory, which forms a square with sides corresponding to F/E (q_2) and R/U (q_3) rotations.

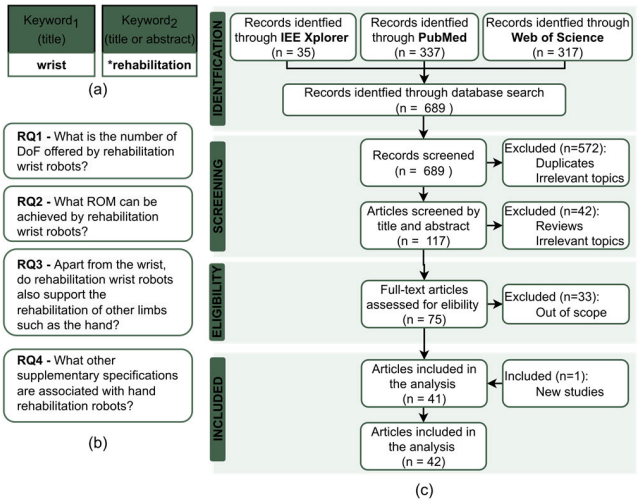

FIGURE 10. Overview of PRISMA flow diagram. (a) Keywords used in the search. (b) Research questions posed. (c) Overview of the selection process.

reference trajectory, an increase in admittance led to a greater discrepancy.

V. DISCUSSION

A literature review using PRISMA (Preferred Reporting Items for Systematic Reviews and Meta-Analyses) was conducted on 22 July 2022 to obtain a comprehensive overview of the mechanical design of wrist rehabilitation robots (Fig. 10). The review was conducted using three databases, namely IEEE Xplorer, Pubmed and Web of Science (WoS), with a predetermined search string consisting of the keywords ''wrist'' in the document title and ''∗rehabilitation'' in the title or abstract (Fig. 10.a). The aim of the systematic review is to gather information about the number of DoFs and ROM offered by rehabilitation wrist robots, the possibility of supporting the rehabilitation of other limbs and other supplementary specifications, such as maximum torque and the inclusion of F/T sensors (Fig. 10.b). The review focused only on journal articles published from 2000 and written in English, excluding commentaries, editorials, or review articles. Additionally, the article must detail the mechanical design of the robot.

An overview of the PRISMA flowchart of the selection process is presented in Fig. 10.c. A total of 689 records were identified through database searches, with 35 from IEEE Xplorer, 317 from WoS, and 337 from PubMed. After

TABLE 5. Comparative analysis of wrist rehabilitation robots: ROM, maximum continuous torque, hand module integration, and f/t sensor capabilities.

	OpenWrist [11]	Lincong Luo [13]	Capello [14]	Wrist Gimbal [16]	POWROBOT [17]	R. Gopura and K. Kiguchi [18]	WRES [21]	**M3Rob device**
ROM P/S (º)	[85, - 85]	[75, – 75]	[80, -80]	[90, -90]	[80, –80]	[60, –80]	[73, -73]	**[90, –90]**
ROM F/E (º)	[60, – 60]	[90, - 90]	[72, -72]	[90, -90]	[80, –80]	[60, –50]	[38, -38]	**[70, –45]**
ROM R/U (º)	[40, – 35]	[35, - 35]	[30, -30]	[30, –30]	[30, -30]	[30, -20]	[20, –20]	**[35, -40]**
Torque P/S (Nm)	3.50	3.05	2.77	2.87	10.46	8.1	6.52	**24.16**
Torque F/E (Nm)	3.60	3.63	1.53	1.76	4.63	1.38	1.62	**43.86**
Torque R/U (Nm)	2.30	3.48	1.63	1.76	3.36	1.38	1.62	**7.85**
Hand module	Yes	No	No	No	No	No	Yes	**Yes**
F/T Sensor	No	No	No	No	Yes	Yes	Yes	**Yes**

FIGURE 11. Schematic diagram of the mechanical configuration of wrist rehabilitation robots considering active DoFs.

a thorough screening process, 572 articles were excluded, either due to duplication or being off-topic (e.g., meta-analysis, systematic reviews, clinical settings, and clinical trials). Subsequently, 117 articles were screened based on title and abstract, and 42 were discarded. Finally, 75 articles were fully read, and 33 were excluded for being out of scope or lacking mechanical specifications. The systematic review ended up with a total of 41 articles, providing a rigorous and valuable resource to compare from a mechanical design point of view the proposed wrist rehabilitation robot with those already presented in existing research studies. One interesting article published after 22 July [21] was identified and included it in the analysis, resulting in a total number of 42.

It was identified that certain articles covered the same device, leading to reducing the total number of wrist rehabilitation robots to 37. Of those, only 16 (43.2%) considered all three DoFs of the wrist. 10 (27.0 %) included only one DoF and 11 (29.7 %) included two DoFs. Additionally, 10 (27 %) of wrist rehabilitation robots also assist the hand movements. Two 3-DoF robots (5.4 %) provide rehabilitation for the elbow, and one of them also assists hand and elbow movements [21]. Fig. 11 shows a schematic diagram of the mechanical configuration of wrist rehabilitation robots only considering the active DoFs.

Regarding passive DoFs, there is a 1-DoF wrist rehabilitation robot that incorporates other limbs (hand, forearm, elbow, and shoulder) by using six different passive components [38]. Other robot offers passive assistance in the MCP movements of the fingers and active assistance in F/E rotations [39]. Another one provides rehabilitation to the hand by assisting reaching movements or to the wrist by assisting in F/E and P/S or R/U rotations [40].

Among the 16 3-DoF wrist rehabilitation robots reviewed, seven are selected based on their wider range of motion in this subset. Table 5 presents an analysis of their ROM, maximum continuous torque, capacity for integrating a hand rehabilitation module, and the availability of F/T sensor.

The M3Rob wrist device stands out as one of the few wrist devices that allow the incorporation of a hand device, while incorporating a 6-axis F/T sensor in the handle and providing a wide ROM. However, for the F/E movement, the provided ROM is slightly smaller. Nevertheless, the device still offers a sufficient range for performing ADLs (see Table 1).

Additionally, the M3Rob wrist device exhibits notably higher torques levels compared to the torque requirements for ADLs, ensuring that the final device does not suffer from insufficient torque production. These torque values surpass the torque capabilities observed in the surveyed robots. Specifically, the provided force ranges between 3.5 and 16.9 times greater than the average torque output of the analyzed robots, with a mean of 5.32±3.07 Nm for P/S, 2.59±1.60 Nm for F/E, and 7.85 Nm R/U, depending on the specific axis of motion. This notable difference is attributed to the exclusion of motor with gearboxes by several authors, resulting in a significant reduction in torque applied to the TCP.

Designing a compact and portable wrist exoskeleton that covers the entire ROM of a healthy wrist, along with the inclusion of a F/T sensor in the handle and allowing for the integration of a hand exoskeleton introduces inherent complexities, as highlighted in the previous literature review. One challenge was to embed a F/T sensor in a removable handle, which can be replaced by a hand exoskeleton for simultaneous hand and wrist rehabilitation. Overcoming this challenge adds complexity to achieving the desired compactness, portability, and necessary ROM, requiring meticulous analysis of upper-limb dimensions [41] to ensure proper device fit and functionality. However, a significant limitation arises in restricting its application to adults, making it unsuitable for pediatric purposes due to the considerably smaller size of children's upper limbs.

VI. CONCLUSION

The development of a highly functional and reliable mechatronic device for wrist and hand rehabilitation is of paramount

importance in the field of robotic assisted physical therapy. The M3Rob wrist device offers a comprehensive solution to address this need. It is a 3-DoF wrist exoskeleton coupled with a force sensor, allowing for the implementation of active therapies that have shown increasing effectiveness in motor recovery.

With a range of motion (ROM) essential for executing activities of daily living (ADLs), the M3Rob boasts P/S capability from −90° to 90°, F/E covering a range from 75 to −45°, and R/U extending from 35° to −40°. Remarkably, the device achieves maximum speeds ranging from 352°/s to 575°/s, surpassing the mandated healthy wrist range of 20-40°/s. Its prismatic joint, with a 28 mm adjustment capability, allows optimal fitting for varying upper-limb sizes in the adult population.

Furthermore, the device's versatility extends with the capacity to integrate the RobHand exoskeleton, enabling simultaneous rehabilitation of both the hand and wrist, further enhancing its practicality and utility. The device's compact and portable design makes it applicable in diverse settings, including hospitals and homes.

A kinematic model of the device has been developed to determine the position and orientation of the terminal control point (TCP), as well as a dynamic model. Experimental assessments were conducted to ascertain static and dynamic friction, yielding values ranging from 0.13-0.49 Nm and 0.13-0.52 Nm, respectively. Comparative analysis with other relevant works highlights the advantages of the proposed design, positioning it as a promising tool in the field of wrist and hand rehabilitation. None of the existing published works offers simultaneous rehabilitation of the 3 DOFs of the wrist, coupled with the ability to concurrently rehabilitate the hand and incorporate a force sensor, all while ensuring achievement of the entire ROM of a healthy wrist. All these attributes are achieved while maintaining a compact and portable design capable of accommodating different arm lengths.

Overall, the M3Rob wrist device represents a significant step forward in the quest for solutions for upper-limb motor recovery. By addressing the challenges associated with wrist and hand rehabilitation, it holds great promise for improving the quality of life for patients who have experienced cerebrovascular accidents. Future research and clinical studies will further validate its efficacy and pave the way for its widespread adoption in rehabilitation practice.

REFERENCES

[1] Z. Gao, Z. Pang, Y. Chen, G. Lei, S. Zhu, G. Li, Y. Shen, and W. Xu, "Restoring after central nervous system injuries: Neural mechanisms and translational applications of motor recovery," *Neurosci. Bull.*, vol. 38, no. 12, pp. 1569–1587, Dec. 2022, doi: 10.1007/s12264-022-00959-x.

[2] V. Ricci and L. Ö. Zçakar, "Wrist and hand," in *Musculoskeletal Diseases 2021–2024: Diagnostic Imaging*, J. Hodler, R. Kubik-Huch, and G. von Schulthess, Eds. Cham, Switzerland: Springer, 2021, pp. 119–139, doi: 10.1007/978-3-030-98256-0_7.

[3] H. Arslan and Í. H. Erdem, "The effect of an intensive hand exercise program on muscle strength and hand functions in patients with rheumatoid arthritis," *Med. Records*, vol. 5, no. 3, pp. 620–626, Sep. 2023, doi: 10.37990/medr.1269997.

[4] I. Vergara, K. Vrotsou, M. Orive, S. Garcia-Gutierrez, N. Gonzalez, C. L. Hayas, and J. M. Quintana, "Wrist fractures and their impact in daily living functionality on elderly people: A prospective cohort study," *BMC Geriatrics*, vol. 16, no. 1, pp. 1–8, Jan. 2016, doi: 10.1186/s12877-015-0176-z.

[5] S. Pradhan, S. Chiu, C. Burton, J. Forsyth, N. Corp, Z. Paskins, D. A. van der Windt, and O. O. Babatunde, "Overall effects and moderators of rehabilitation in patients with wrist fracture: A systematic review," *Phys. Therapy*, vol. 102, no. 6, pp. 1–11, Jun. 2022, doi: 10.1093/ptj/pzac032.

[6] C. Bütefisch, H. Hummelsheim, P. Denzler, and K.-H. Mauritz, "Repetitive training of isolated movements improves the outcome of motor rehabilitation of the centrally paretic hand," *J. Neurol. Sci.*, vol. 130, no. 1, pp. 59–68, May 1995, doi: 10.1016/0022-510x(95)00003-k.

[7] A. Gupta and M. K. O'Malley, "Design of a haptic arm exoskeleton for training and rehabilitation," *IEEE/ASME Trans. Mechatronics*, vol. 11, no. 3, pp. 280–289, Jun. 2006, doi: 10.1109/TMECH.2006.875558.

[8] A. Gupta, M. K. O'Malley, V. Patoglu, and C. Burgar, "Design, control and performance of RiceWrist: A force feedback wrist exoskeleton for rehabilitation and training," *Int. J. Robot. Res.*, vol. 27, no. 2, pp. 233–251, Feb. 2008, doi: 10.1177/0278364907084261.

[9] J. A. French, C. G. Rose, and M. K. O. Malley, "System characterization of MAHI Exo-II: A robotic exoskeleton for upper extremity rehabilitation," in *Proc. ASME Dyn. Syst. Control Conf. (DSCC)*, Oct. 2014, pp. 1–5, doi: 10.1115/DSCC2014-6267.

[10] A. U. Pehlivan, F. Sergi, A. Erwin, N. Yozbatiran, G. E. Francisco, and M. K. O'Malley, "Design and validation of the RiceWrist-S exoskeleton for robotic rehabilitation after incomplete spinal cord injury," *Robotica*, vol. 32, no. 8, pp. 1415–1431, Dec. 2014, doi: 10.1017/s0263574714001490.

[11] E. Pezent, C. G. Rose, A. D. Deshpande, and M. K. O'Malley, "Design and characterization of the OpenWrist: A robotic wrist exoskeleton for coordinated hand-wrist rehabilitation," in *Proc. Int. Conf. Rehabil. Robot. (ICORR)*, Jul. 2017, pp. 720–725, doi: 10.1109/ICORR.2017.8009333.

[12] C. G. Rose, F. Sergi, Y. Yun, K. Madden, A. D. Deshpande, and M. K. O'Malley, "Characterization of a hand-wrist exoskeleton, READAPT, via kinematic analysis of redundant pointing tasks," in *Proc. IEEE Int. Conf. Rehabil. Robot. (ICORR)*, Aug. 2015, pp. 205–210, doi: 10.1109/ICORR.2015.7281200.

[13] L. Luo, L. Peng, Z. Hou, and W. Wang, "Design and control of a 3-DOF rehabilitation robot for forearm and wrist," in *Proc. 39th Annu. Int. Conf. IEEE Eng. Med. Biol. Soc. (EMBC)*, Jul. 2017, pp. 4127–4130, doi: 10.1109/EMBC.2017.8037764.

[14] L. Cappello, S. Contu, N. Elangovan, S. Khosravani, J. Konczak, and L. Masia, "Evaluation of wrist joint proprioception by means of a robotic device," in *Proc. 11th Int. Conf. Ubiquitous Robots Ambient Intell. (URAI)*, Nov. 2014, pp. 531–534, doi: 10.1109/URAI.2014.7057383.

[15] L. Masia, M. Casadio, P. Giannoni, G. Sandini, and P. Morasso, "Performance adaptive training control strategy for recovering wrist movements in stroke patients: A preliminary, feasibility study," *J. Neuroeng. Rehabil.*, vol. 6, no. 1, pp. 1–11, Dec. 2009, doi: 10.1186/1743-0003-6-44.

[16] J. A. Martinez, P. Ng, S. Lu, M. S. Campagna, and O. Celik, "Design of wrist gimbal: A forearm and wrist exoskeleton for stroke rehabilitation," in *Proc. IEEE 13th Int. Conf. Rehabil. Robot. (ICORR)*, Jun. 2013, pp. 1–6, doi: 10.1109/ICORR.2013.6650459.

[17] U. Mayetin and S. Kucuk, "Design and experimental evaluation of a low cost, portable, 3-DOF wrist rehabilitation robot with high physical human–robot interaction," *J. Intell. Robotic Syst.*, vol. 106, no. 3, p. 65, Nov. 2022, doi: 10.1007/s10846-022-01762-6.

[18] R. A. R. C. Gopura and K. Kiguchi, "Development of an exoskeleton robot for human wrist and forearm motion assist," in *Proc. 2nd Int. Conf. Ind. Inf. Syst.*, Aug. 2007, pp. 535–540, doi: 10.1109/ICIINFS.2007.4579235.

[19] N. Omarkulov, K. Telegenov, M. Zeinullin, I. Tursynbek, and A. Shintemirov, "Preliminary mechanical design of NU-Wrist: A 3-DOF self-aligning wrist rehabilitation robot," in *Proc. 6th IEEE Int. Conf. Biomed. Robot. Biomechatronics (BioRob)*, Jun. 2016, pp. 962–967, doi: 10.1109/BIOROB.2016.7523753.

[20] Z. Qian and Z. Bi, "Recent development of rehabilitation robots," *Adv. Mech. Eng.*, vol. 7, no. 2, Jan. 2015, Art. no. 563062, doi: 10.1155/2014/563062.

[21] D. Buongiorno, E. Sotgiu, D. Leonardis, S. Marcheschi, M. Solazzi, and A. Frisoli, "WRES: A novel 3 DoF WRist ExoSkeleton with tendon-driven differential transmission for neuro-rehabilitation and teleoperation," *IEEE Robot. Autom. Lett.*, vol. 3, no. 3, pp. 2152–2159, Jul. 2018, doi: 10.1109/LRA.2018.2810943.

[22] A. A. Blank, J. A. French, A. U. Pehlivan, and M. K. O'Malley, "Current trends in robot-assisted upper-limb stroke rehabilitation: Promoting patient engagement in therapy," *Current Phys. Med. Rehabil. Rep.*, vol. 2, no. 3, pp. 184–195, Sep. 2014, doi: 10.1007/s40141-014-0056-z.
[23] Z. Yue, X. Zhang, and J. Wang, "Hand rehabilitation robotics on poststroke motor recovery," *Behavioural Neurol.*, vol. 2017, pp. 1–20, Nov. 2017, doi: 10.1155/2017/3908135.
[24] J. C. Perry, J. M. Powell, and J. Rosen, "Isotropy of an upper limb exoskeleton and the kinematics and dynamics of the human arm," *Appl. Bionics Biomech.*, vol. 6, no. 2, pp. 175–191, Jul. 2009, doi: 10.1080/11762320902920575.
[25] J. G. Andrews and Y. Youm, "A biomechanical investigation of wrist kinematics," *J. Biomech.*, vol. 12, no. 1, pp. 83–93, Jan. 1979.
[26] Y.-Y. Su, Y.-L. Yu, C.-H. Lin, and C.-C. Lan, "A compact wrist rehabilitation robot with accurate force/stiffness control and misalignment adaptation," *Int. J. Intell. Robot. Appl.*, vol. 3, no. 1, pp. 45–58, Mar. 2019, doi: 10.1007/s41315-019-00083-6.
[27] K. Nizamis, N. Rijken, A. Mendes, M. Janssen, A. Bergsma, and B. Koopman, "A novel setup and protocol to measure the range of motion of the wrist and the hand," *Sensors*, vol. 18, no. 10, p. 3230, Sep. 2018, doi: 10.3390/s18103230.
[28] J. C. Perry, J. Rosen, and S. Burns, "Upper-limb powered exoskeleton design," *IEEE/ASME Trans. Mechatronics*, vol. 12, no. 4, pp. 408–417, Aug. 2007, doi: 10.1109/TMECH.2007.901934.
[29] J. Ryu, W. P. Cooney, L. J. Askew, K.-N. An, and E. Y. S. Chao, "Functional ranges of motion of the wrist joint," *J. Hand Surg.*, vol. 16, no. 3, pp. 409–419, May 1991, doi: 10.1016/0363-5023(91)90006-w.
[30] S. J. Bae, S. H. Jang, J. P. Seo, and P. H. Chang, "The optimal speed for cortical activation of passive wrist movements performed by a rehabilitation robot: A functional NIRS study," *Frontiers Human Neurosci.*, vol. 11, pp. 1–7, Apr. 2017, doi: 10.3389/fnhum.2017.00194.
[31] B. D. P. Correa, "Diseño del sistema mecánico de un equipo para rehabilitación de la muñeca usando mecanismos paralelos," Dept. Sci. Eng., Pontificia Universidad Católica del Perú, Perú, Tech. Rep. 93, 2017.
[32] G. Xu, X. Gao, L. Pan, S. Chen, Q. Wang, B. Zhu, and J. Li, "Anxiety detection and training task adaptation in robot-assisted active stroke rehabilitation," *Int. J. Adv. Robotic Syst.*, vol. 15, no. 6, Nov. 2018, Art. no. 172988141880643, doi: 10.1177/1729881418806433.
[33] R. M. Patterson, C. L. Nicodemus, S. F. Viegas, K. W. Elder, and J. Rosenblatt, "High-speed, three-dimensional kinematic analysis of the normal wrist," *J. Hand Surg.*, vol. 23, no. 3, pp. 446–453, May 1998, doi: 10.1016/s0363-5023(05)80462-9.
[34] A. Cisnal, V. Moreno-SanJuan, J. C. Fraile, J. P. Turiel, E. de-la-Fuente, and G. Sánchez-Brizuela, "Assessment of the patient's emotional response with the RobHand rehabilitation platform: A case series study," *J. Clin. Med.*, vol. 11, no. 15, p. 4442, Jul. 2022, doi: 10.3390/jcm11154442.
[35] P. Barria, M. Riquelme, H. Reppich, A. Cisnal, J.-C. Fraile, J. Pérez-Turiel, D. Sierra, R. Aguilar, A. Andrade, and C. Nuñez-Espinosa, "Hand rehabilitation based on the RobHand exoskeleton in stroke patients: A case series study," *Frontiers Robot. AI*, vol. 10, pp. 1–15, Mar. 2023, doi: 10.3389/frobt.2023.1146018.
[36] V. Moreno-SanJuan, A. Cisnal, J.-C. Fraile, J. Pérez-Turiel, and E. de-la-Fuente, "Design and characterization of a lightweight underactuated RACA hand exoskeleton for neurorehabilitation," *Robot. Auto. Syst.*, vol. 143, Sep. 2021, Art. no. 103828, doi: 10.1016/j.robot.2021.103828.
[37] M. Mihelj and J. Podobnik, *Haptics for Virtual Reality and Teleoperation*, vol. 64, S. G. Tzafestas, Ed. Dordrecht, The Netherlands: Springer, 2012, doi: 10.1007/978-94-007-5718-9.
[38] K. X. Khor, P. J. H. Chin, C. F. Yeong, E. L. M. Su, A. L. T. Narayanan, H. A. Rahman, and Q. I. Khan, "Portable and reconfigurable wrist robot improves hand function for post-stroke subjects," *IEEE Trans. Neural Syst. Rehabil. Eng.*, vol. 25, no. 10, pp. 1864–1873, Oct. 2017, doi: 10.1109/TNSRE.2017.2692520.
[39] N. Singh, M. Saini, S. Anand, N. Kumar, M. V. P. Srivastava, and A. Mehndiratta, "Robotic exoskeleton for wrist and fingers joint in post-stroke neuro-rehabilitation for low-resource settings," *IEEE Trans. Neural Syst. Rehabil. Eng.*, vol. 27, no. 12, pp. 2369–2377, Dec. 2019, doi: 10.1109/TNSRE.2019.2943005.
[40] J. Oblak, I. Cikajlo, and Z. Matjacic, "Universal haptic drive: A robot for arm and wrist rehabilitation," *IEEE Trans. Neural Syst. Rehabil. Eng.*, vol. 18, no. 3, pp. 293–302, Jun. 2010, doi: 10.1109/TNSRE.2009.2034162.
[41] A. R. Tiley, "The measure of man and woman: Human factors in design," in *Whitney Library Design*, R. de Alba, Ed. New York, NY, USA: Henry Dreyfuss Associates, 1993, p. 96.

GONZALO ALONSO-LINAJE received the B.S. degree in mechanical engineering and the M.S. degree in industrial engineering from the University of Valladolid, Valladolid, Spain, in 2019 and 2022, respectively. Since 2021, he has been with the Advanced Production Technologies Institute (ITAP), University of Valladolid, as a Contract Researcher. His current research interest includes robotic neuromotor rehabilitation platforms.

ANA CISNAL (Graduate Student Member, IEEE) received the Ph.D. degree in industrial engineering from the University of Valladolid, Spain, in 2023. She participated in quality internships with the CARTIF Technology Center, Spain; Fraunhofer IBMT, Germany; and Sensory-Motor Systems Lab, ETH Zürich, Switzerland. Since 2017, she has been engaged in research activities with the Medical Robotics Group, Advanced Production Technologies Institute (ITAP). Her current research interest includes development of control strategies for robotic neuromotor rehabilitation platforms.

JUAN CARLOS FRAILE received the Ph.D. degree in control engineering from the Faculty of Engineering, University of Valladolid, Spain, in 1987. Since 1992, he has been an Associate Professor of control and robotics with the Faculty of Engineering, University of Valladolid. In 1998, he was a Visiting Professor with the Institute of Complex Engineering Systems (ICES), Carnegie Mellon University, Pittsburgh, PA, USA. He is currently the Leader of the ITAP-Medical Robotics Group, University of Valladolid. His current research interests include rehabilitation robotics and robots for surgery.

JAVIER P. TURIEL received the Ph.D. degree in control engineering from the University of Valladolid, Spain, in 1994.

In 1999, he was a Visiting Professor with the Electrical Engineering and Computer Science Department (EECS), University of Michigan, Ann Arbor, MI, USA. He was the Head of the Biomedical Engineering Division, CARTIF Technology Center, from 2000 to 2014. He is currently an Associate Professor with the Department of Systems Engineering, University of Valladolid. He is also a member with the Medical Robotics Group, Advanced Production Technologies Institute (ITAP). His research interests include surgical and rehabilitation robots.